

Well-Controlled Formation of Polymeric Micelles with a Nanosized Aqueous Core and Their Applications as Nanoreactors

Fei Cheng,[†] Xiaogang Yang,[†] Huisheng Peng,[‡] Daoyong Chen,^{*,†} and Ming Jiang[†]

Key Laboratory of Molecular Engineering of Polymers of the Ministry of Education, Department of Macromolecular Science, Fudan University, Shanghai 200433, China, and Los Alamos National Laboratory, P.O. Box 1663, Los Alamos, New Mexico 87545

Received March 29, 2007; Revised Manuscript Received August 1, 2007

ABSTRACT: Polymeric micelles with a polystyrene (PS) shell and a protonated poly(4-vinylpyridine) (P4VP)/water core were readily prepared via diffusion of HCl and water from the top aqueous phase containing HCl (pH = 1) into the bottom phase of the PS-*b*-P4VP solution in chloroform. The resultant protonation of the pyridine units of the P4VP block drove the micellization. Meanwhile, due to the high polarity of the core, water molecules also diffused through the chloroform medium into the core. ¹H NMR characterizations demonstrate that at the early stage, the water molecules in the core are the bound and intermediate water; longer diffusion times resulted in the appearance of free water molecules coexisting with the bound and intermediate water in the core. Thus, polymeric micelles with an aqueous core (PMACs) were formed. The process of forming PMACs is well-controllable, and the stability of PMACs in chloroform is high. These characteristics make PMACs promising as nanoreactors to prepare inorganic nanoparticles or for other applications based on the nanosized aqueous core. Similar to reverse mini- and microemulsion systems, the same PMACs can load a large variety of water-soluble inorganic species and be used to prepare various inorganic nanoparticles within the core. Meanwhile, similar to block copolymer micelles, the soluble shell of PMACs can provide a good solubility for the inorganic nanoparticles formed in the core. Therefore, when used as nanoreactors to prepare inorganic nanoparticles, PMACs can combine the advantages of reverse emulsion systems and polymeric micelles dispersed in a low polar solvent. Herein, PMACs with a PS shell and a protonated P4VP/water core prepared in chloroform were used as nanoreactors to prepare various inorganic nanoparticles, such as silica, Fe(SCN)²⁺, AgCl, and Ag₂CINO₃. The formed inorganic nanoparticles were encapsulated in the core and stabilized in chloroform by the soluble PS shell.

Introduction

Polymeric micelles (PMs)^{1–8} with a high-polarity core dispersed in a low-polarity solvent and reverse mini- or microemulsions (REs)^{9–13} have been used as nanoreactors to prepare inorganic nanoparticles. The polar core of PMs and the nano- or micro-sized droplets of REs can collect desirable inorganic species. In addition, the sharp contrast in polarity between the polar core or the nanodroplet and the low-polarity medium can localize an inorganic reaction and provide facile control over the size and size distribution of the formed inorganic nanoparticles. However, as nanoreactors, both PMs and REs have their advantages and disadvantages. In most cases, PMs load inorganic precursors based on electrostatic^{14–17} or coordinating^{18–20} interactions. Only those strongly interacting with the core components can be loaded. However, the resultant inorganic nanoparticles are usually well-dispersed in solutions due to the PM shell composed of soluble polymer chains, which greatly extends the applications of the inorganic nanoparticles. In principle, the same REs can load all water-soluble inorganic precursors, whereas the resultant inorganic nanoparticles are not so well-stabilized in solutions as those formed in PMs.²¹ Ideally, the same polymeric micelles with an aqueous core (PMACs) can load a wide variety of inorganic precursors and stabilize the produced inorganic nanoparticles (i.e., PMACs combine the advantages of PMs and REs when used as nanoreactors). Recently, Scott et al.^{22,23} reported the preparation of polymeric

nanoparticles with an aqueous core by conducting an alternative copolymerization of a hydrophilic monomer and a hydrophobic monomer at the water/oil interface of a reverse emulsion. Jones et al.²⁴ constructed nanocages with alkylated star-shaped poly-(glycerol methacrylate) polymers for encapsulating various peptides/proteins.

Herein, we introduce a robust and well-controlled pathway to prepare PMACs with a PS shell and a protonated P4VP/water core in chloroform and their applications as a versatile nanoreactor to synthesize inorganic nanoparticles. Since the loading of inorganic precursors is based on their water solubility, many water-soluble species can be loaded in the aqueous core. The transfer of inorganic precursors through chloroform into the aqueous cores is remarkably facilitated by a small amount of HCl molecules in chloroform. Various inorganic nanoparticles, such as SiO₂, Fe(SCN)²⁺, AgCl, and Ag₂CINO₃, can be prepared in PMACs and further stabilized by the PS shell in the solution.

Experimental Procedures

Materials. Block copolymer PS₁₉₇-*b*-P4VP₃₄₃ (the subscripts indicate the average number of repeating units of respective blocks) used in this study was purchased from Polymer Source Inc. The M_n of the PS and P4VP blocks are 20 500 and 36 000 g/mol, respectively. The M_n , M_w , and polydispersity of the block polymers are 56 500 g/mol, 61 000 g/mol, and 1.08, respectively. Tetraethoxysilane (TEOS) with a purity of 98% was purchased from Alfa Aesar. Deuterated chloroform (D, 99.8%) with 0.03% (v/v) TMS as an internal reference is a commercial product from CIL. The other chemicals are of analytical grade and used without further purification.

* Corresponding author. E-mail: chendy@fudan.edu.cn.

[†] Fudan University.

[‡] Los Alamos National Laboratory.

Construction of the Biphasic System and the Protonation-Induced Micellization of PS-*b*-P4VP in the Chloroform Phase. The PS₁₉₇-*b*-P4VP₃₄₃ copolymer was dissolved in chloroform or deuterated chloroform (for ¹H NMR characterizations) at a concentration of 2.0 mg/mL for 24 h. A total of 10.0 mL of the resultant polymer solution was transferred into a columnar vial (the inner diameter was 2 cm). Then, 5.0 mL of a HCl aqueous solution at pH 1 was added carefully on top of the polymer solution under mild magnetic stirring (ca. 100 rpm) to form a top aqueous phase. The changes in the chloroform phase at different times were tracked by dynamic light scattering (DLS) and ¹H NMR.

Effect of HCl on the Transfer of Inorganic Species through the Chloroform Phase. We designed simple experiments to demonstrate that the transfer of inorganic compounds from the top aqueous phase through chloroform can be accelerated by HCl. In the experiments, a piece of test paper responsive to an inorganic compound was placed at the bottom of a vial. CHCl₃ was added to cover the test paper with a 2 cm thick CHCl₃ layer. Then, the aqueous solution of the inorganic compound was added carefully on top of the chloroform phase. The biphasic system was set still. The transfer speed of the inorganic compound through the chloroform phase to reach the test paper at the bottom of the vial was evaluated by the time taken for the color change of the test paper. The effect of HCl can be demonstrated by comparing the transfer speed measured for the inorganic compound dissolved in pH 1 HCl aqueous solution with that dissolved in neutral water.

Preparation of Inorganic Nanoparticles Using PMACs as Nanoreactors. A total of 120 h after the formation of the biphasic system of the pH 1 HCl aqueous solution/PS-*b*-P4VP chloroform solution, the top aqueous phase was discarded, and the PMAC solution in chloroform was used to prepare inorganic nanoparticles. (1) For the preparation of SiO₂ nanoparticles within the aqueous cores of PMACs, 0.04 mL of TEOS was syringed into 5.0 mL of the PMAC solution in chloroform. The mixture was magnetically stirred for 30 h. (2) For preparing nanoparticles of Fe³⁺/(SCN)⁻ complexes in PMACs, a triphasic system was constructed via the following procedure: 3.5 mL of an aqueous solution saturated with FeCl₃ (the concentration was 0.74 g/mL, and the density was higher than that of chloroform), 3.5 mL of the PMAC chloroform solution (the concentration of the copolymer was 2.0 mg/mL), and 3.5 mL of NH₄SCN aqueous solution at a concentration of 20 mg/mL containing HCl (pH = 1) were added into a vial carefully and sequentially. In a control experiment, a similar triphasic system was constructed with 3.5 mL of the aqueous solution saturated with FeCl₃, 3.5 mL of chloroform (without PMACs), and 3.5 mL of the NH₄SCN aqueous solution at 20 mg/mL containing HCl (pH = 1). (3) AgCl nanoparticles were prepared by mixing 20 mg of AgNO₃ with 5.0 mL of the PMAC solution at a concentration of the block copolymer of 2.0 mg/mL under mild ultrasonic and ambient temperature (~20 °C) for half an hour. Ag⁺ introduced into the cores can react with Cl⁻ (as the counterions of protonated pyridine units) to form AgCl. After setting the mixture solution still for minutes, the extra AgNO₃ outside the core precipitated out of the solution and was removed. (4) After exposing the PMAC solution containing AgCl nanoparticles and AgNO₃ in the aqueous core to broad-spectrum ultraviolet rays for 5 min, Ag₂CINO₃ nanoparticles and a small amount of Ag were formed within the core.

Characterization. Dynamic Light Scattering (DLS). A commercial laser light scattering (LLS) spectrometer (Malvern Autosizer 4700) equipped with a multi- τ digital time correlation (Malvern PCS7132) and a solid-state laser (ILT 5500QSL, output power = 100 mW at $\lambda_0 = 514.5$ nm) as a light source was used. The line-width distribution $G(\Gamma)$ can be calculated from the Laplace inversion of the intensity time correlation function into a transitional diffusion coefficient distribution $G^{(2)}(q, t)$.^{25,26} The inversion was carried out by the CONTIN program supplied with a Malvern PCS7132 digital time correlator. The average hydrodynamic radius (R_h) of the nanoparticles was calculated using the Stokes–Einstein equation, $R_h = k_B T / 6\pi\eta D$, where k_B , T , and η are the Boltzmann constant, the absolute temperature, and the solvent viscosity, respectively.

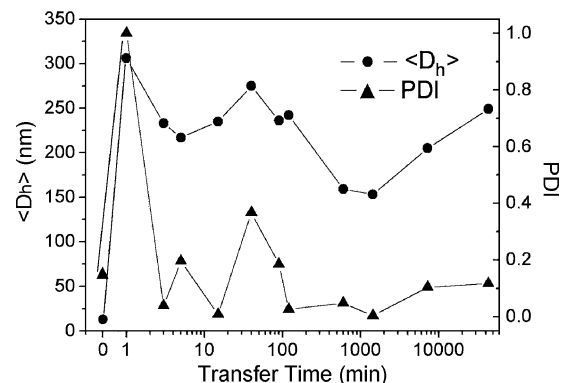


Figure 1. DLS characterization data of aggregates formed in the PS-*b*-P4VP chloroform solution at different transfer times (t). $\langle D_h \rangle$ is the hydrodynamic diameter of the aggregates, and PDI (polydispersity index) is the size distribution.

All the DLS measurements were conducted at 25.0 °C and at a scattering angle of 90°.

¹H NMR Measurements. The ¹H NMR measurements were performed on a Bruker DMX500 spectrometer in deuterated chloroform with TMS as an internal reference.

TEM and Energy-Dispersive X-ray (EDX) Spectroscopy. TEM and EDX were conducted on a Philips CM 120 electron microscope at an acceleration voltage of 80 kV. The samples for the TEM observations were prepared by dropping a droplet of micelle solutions on a copper grid. The excess solution was wicked away immediately. Sample drying was performed in a desiccator to prevent the samples from absorbing water.

UV–vis Spectroscopy was carried out on a Lambda 35 UV–vis absorption spectrometer from PerkinElmer.

Results and Discussion

Micellization of PS-*b*-P4VP and Formation of PMACs.

The biphasic system in the present study was composed of 5.0 mL of a pH 1 HCl aqueous solution as the top phase and 10.0 mL of a 2.0 mg/mL PS-*b*-P4VP/CHCl₃ solution as the bottom phase. The solutions were held in a columnar vial with an inner diameter of 2.0 cm and gently stirred (ca. 100 rpm) by a small magnetic bar (the magnetic bar is 2.0 mm in diameter and 6.5 mm in length) at the bottom. Under such gentle stirring, the water/chloroform interface was flat, and no disturbance at the interface due to the stirring can be observed. It is known that PS-*b*-P4VP can be molecularly dispersed in chloroform. However, the chloroform phase became bluish in minutes after the formation of the biphasic system. In addition, the scattering light intensity of the polymer solution increased gradually, indicating the formation of aggregates in the chloroform phase, while the top aqueous phase still remained clear. The aggregation of PS₁₉₇-*b*-P4VP₃₄₃ in the chloroform phase was tracked by DLS at different transfer times (t) (Figure 1; timing began upon adding the pH 1 HCl aqueous solution on the top of the chloroform solution). From Figure 1, we can see that when $t = 1$ min, large aggregates (the z -average hydrodynamic diameter $\langle D_h \rangle$ of 306 nm) with a wide size distribution (the polydispersity index ($\mu_2/(\Gamma)^2$) (PDI) of 1.0) were detected. The light scattering intensity of the aggregates was very low. The large size, wide size distribution and low light scattering intensity indicate that the aggregates formed at $t = 1$ min are the result of an anomalous micellization.^{27,28} This conclusion is also supported by the TEM observation (S1, Supporting Information (SI)). The $\langle D_h \rangle$ value of the aggregates rapidly decreased to 233 nm at $t = 3$ min, and the size distribution became narrower (PDI = 0.039). When $3 \text{ min} \leq t \leq 2 \text{ h}$, the $\langle D_h \rangle$ value fluctuated between 217 and

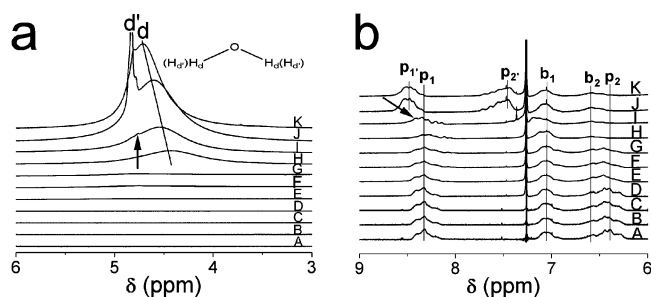


Figure 2. ^1H NMR spectra of the micelle solutions in CDCl_3 at different transfer times (t): (A: 1 min; B: 3 min; C: 5 min; D: 15 min; E: 40 min; F: 90 min; G: 2 h; H: 10 h; I: 24 h; J: 120 h; and K: 720 h). (a) From 6 to 3 ppm and (b) from 9 to 6 ppm.

275 nm. When $t = 10$ and 24 h, the $\langle D_h \rangle$ value decreased again to 159 and 153 nm, respectively. Afterward, the $\langle D_h \rangle$ value gradually increased until $t = 720$ h, and then no remarkable changes in the size or size distribution were observed.

To study the micellization mechanism of PS-*b*-P4VP in the chloroform phase, we first demonstrated that HCl could diffuse from the top aqueous phase into the chloroform phase by a simple experiment. A piece of pH test paper was placed at the bottom of a vial, followed by the addition of a 2 cm thick chloroform layer to cover the test paper. Then, the pH 1 HCl aqueous solution was dropped carefully on the top of the chloroform layer. The pH test paper turned red in minutes after formation of the pH 1 HCl aqueous solution/chloroform biphasic system. Obviously, in the biphasic system of the pH 1 HCl aqueous solution/PS-*b*-P4VP chloroform solution, HCl diffused into chloroform solution to protonate the pyridine units. The protonated pyridine units with a high polarity were insoluble in chloroform and aggregated to drive the micellization of the block copolymer, forming micelles with a PS shell and protonated P4VP core. This is consistent with results of our previous studies that low molecular weight acids can interact with the pyridine units and induce the micellization of PS-*b*-P4VP in chloroform.^{29–32} In a control experiment, where the top pH 1 HCl aqueous phase was replaced by neutral deionized water, no aggregates were detected by DLS in either the top phase or the chloroform solution in weeks.

Eisenberg et al. reported that in the mixture of polymeric micelles in a low polar solvent with a small amount of water, water was molecularly solubilized in the bulk solvent phase and existed in the core of polymeric micelles.³³ In the present study, due to the high polarity of the cores formed by the protonated or partially protonated P4VP block chains, water can diffuse from the top aqueous phase into the core of the micelles. The process of the water diffusion into the cores was tracked by ^1H NMR. As shown in Figure 2a, the ^1H NMR spectra of the block copolymer in CDCl_3 at $t \geq 40$ min (spectra E to ~K in Figure 2a) show a broad peak d at chemical shift (δ) 4.4–4.7 ppm (peak d in spectra E–G can be seen when the spectra are enlarged; relative intensities of peak d were given by the instrument). The water molecularly solubilized in the CDCl_3 bulk solution phase was limited to a small amount and gave a sharp peak at δ of 1.59 ppm in the ^1H NMR spectra (S2, SI); the water droplets in chloroform give a sharp peak at 4.6–4.8 ppm (it is imaginable that the individual water molecules in a water droplet are surrounded by water, so they are in a polar environment; S3, SI). In the present study, the biphasic system was gently stirred to accelerate the diffusion of the species in the chloroform phase without considerably shearing the water/chloroform interface, as mentioned before. We believe that water only molecularly diffused from the top aqueous phase into the

Table 1. Summary of Relative Water Amount at Different Transfer Times (t)

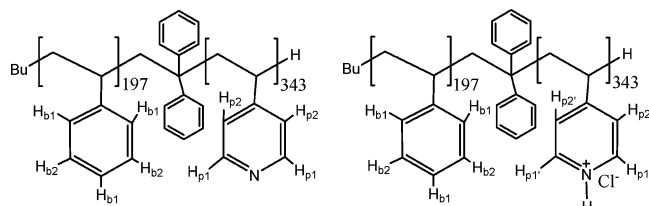
t	M_1^a	M_2^b
1 min	ND ^c	ND
3 min	ND	ND
5 min	ND	ND
15 min	ND	ND
40 min	0.39	2.27
90 min	0.86	5.00
2 h	0.97	5.70
10 h	2.93	17.13
24 h	4.35	25.33
120 h	9.86	57.39
720 h	10.97	63.88

^a Mass ratio of water in the core to 4VP repeating units. ^b Molar ratio of water in the core to pyridine units. ^c Water molecules diffusing into the core at the early stage are bound water in a small amount that may aggregate together with the protonated pyridine units. During the early stage, the mobility of the bound water should be restricted seriously, so their signal is remarkably widened. The widening and the small amount make their signal undetectable by liquid ^1H NMR. However, during the late stage, the bound water in the cores of PMACs can be detected by ^1H NMR since the protonated P4VP chains were then in a solubilized state in the aqueous cores.

chloroform phase. The wide peak at 4.4–4.7 ppm should be associated with water molecules diffused into the high polar core of the as-formed micelles. The remarkable widening of the water signal indicates a strong interaction between the water molecules and the core component. It is noted that at $t \geq 24$ h, a sharp peak d' appears at 4.8 ppm (spectra I–K in Figure 2a). This sharp peak shows characters (i.e., the width and chemical shift) identical to those of the ^1H NMR signal of H_2O solubilized in D_2O (S3, SI). On the basis of these characters and the reported results,³⁴ peak d' should be attributed to the free water existing in the cores. According to Jhon and Andrade,³⁵ water molecules in a hydrogel can be classified as the bound water, intermediate water, and free water (explanation of these three states of water are given in S4, SI). The wide peak d, which appeared before the appearance of peak d', should be attributed to the bound water and intermediate water. Naturally, the water molecules diffused into the core at the early period of the water diffusion are strongly bound to the protonated pyridine units; after the complete occupation of the protonated pyridine units by bound water, the intermediate water comes into the core, rapidly exchanging with the bound water and giving the wide peak d in spectra E–H in Figure 2a. Afterward, with the diffusion of additional water into the core, the signal of free water d' was detected. The weight ratios and molar ratios of water to the pyridine units of the P4VP blocks at different t values, which were evaluated based on the area ratios of the respective peaks in the corresponding spectrum (S5, SI), are summarized in Table 1. From Table 1, we can see that the amount of the water detected in the polymeric micelle solution increases steadily. When $t = 720$ h, the weight ratio and molar ratio of the water to the 4VP repeating units reached 10.97 and 63.88, respectively. This indicates that the as-formed micelles can encapsulate a large amount of water in the cores. Obviously, the core containing so large an amount of water may be considered to be a droplet of aqueous solution of the protonated P4VP blocks.

In our previous studies,^{29–32} liquid ^1H NMR characterization was used to determine the core–shell structure of block copolymer micelles. As the core of the micelles is in an aggregated state, the signals of the core-forming block chains are weakened or even disappear, depending on the density of the cores. In the present study, the change in the structure of

Scheme 1. Chemical Structures of Block Copolymer before and after Protonation and Assignments of H Atoms of the Block Copolymer



the cores during protonation and water diffusion was also studied by liquid ^1H NMR.

The chemical structures of the block copolymer before and after protonation, and the assignments of the H atoms in ^1H NMR spectra, are given in Scheme 1. The spectra of the block copolymer in the CDCl_3 phase at different t values are presented in Figure 2b. In Figure 2b, peaks p_1 , p_2 , b_1 , and b_2 are assigned to H_{p1} and H_{p2} of the pyridine rings and H_{b1} and H_{b2} of the benzene rings, respectively; peaks p_1' and p_2' are related to, respectively, $\text{H}_{p1'}$ and $\text{H}_{p2'}$ in the protonated pyridine units in the aqueous core. In the present study, it is found that the area ratio of peak p_1 (associated to H_{p1} of the pyridine units, Scheme 1) to peak b_1 (related to H_{b1} of the benzene rings) decreases gradually from 1.16 to 0.64 when t increases from 0 to 10 h (spectra A–H in Figure 2b). The decrease in the relative intensity of the pyridine signals indicates that the cores of the as-formed polymeric micelles should be composed of P4VP block chains. This is consistent with the mechanism of micellization mentioned previously that the solubility decrease of the P4VP blocks due to the protonation drives the micellization of the block copolymer. However, protonated pyridine signals did not appear until $t \geq 24$ h, although water signals were detected at $t \geq 40$ min. This may be due to the fact that the protonated pyridine units are connected by P4VP chains and have less mobility than the bound and intermediate water molecules. The protonated pyridine signals were detected when $t \geq 24$ h and the signal of free water appears. The simultaneous appearance of free water and the protonated pyridine signals are indicated by the two arrows in spectrum I (Figure 2a,b). The appearance of the free water indicates that the core begins to become an aqueous solution of the protonated P4VP block chains. In this aqueous solution, the protonated pyridine units begin to be movable so that they can be detected by liquid ^1H NMR. It is noted that when $t \geq 24$ h, the broad peak d (the signal of the bound and intermediate water) still exists and keeps shifting to low field with the increase of t ; its intensity increases with t as well. This should be due to the proton exchange between water molecules in the three states and the change in the structure and polarity of the cores. When $t \geq 120$ h, the area ratio of peak p_1' (signal of $\text{H}_{p1'}$ of the protonated pyridine units) to peak b_1 (signal of H_{b1} of the benzene rings) is close to that calculated according to the lengths of the two blocks. In other words, when $t \geq 120$ h, all the pyridine units are protonated, and all the protonated pyridine units are detectable by liquid ^1H NMR. This supports our speculation that the core of the micelles encapsulates so large an amount of water that it should be regarded as an aqueous solution of the protonated P4VP block chains. Thus, polymeric micelles with an aqueous core (PMACs) were formed. The relative water content did not change remarkably from 120 to 720 h. From the previous description, we can see that the processes of forming PMACs are very steady and can be well-controlled.

It is known that in a selective solvent of a block copolymer, the size of the resultant micelles is determined by the structure

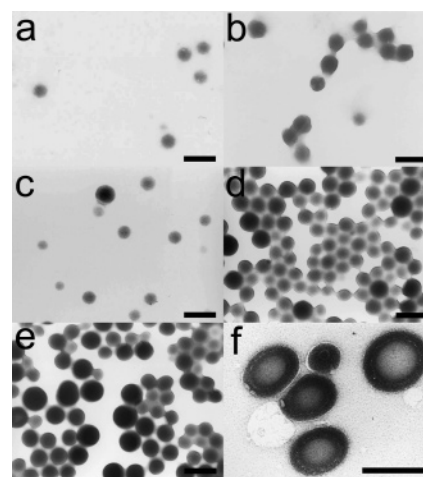


Figure 3. TEM images of micelles at different transfer times (a: 3 min; b: 15 min; c: 10 h; d: 24 h; and e: 120 h) and the TEM image of PMACs (f: $t = 120$ h) cross-linked by bivalent $\text{S}_2\text{O}_8^{2-}$ ions. All the scale bars are 200 nm in length.

parameters of the block copolymer.³⁶ However, in the present study, DLS measurements indicate that the $\langle D_h \rangle$ value of the polymeric micelles formed at $t < 10$ h or $t \geq 120$ h is above 200 nm (Figure 1), much larger than that of polymeric micelles formed by a block copolymer in its selective solvent predicted by a scaling law.³⁶ This reflects the swollen structure of the core of the polymeric micelles in the present study. Our ^1H NMR characterization exhibits that when $t < 10$ h, the core was swollen by CDCl_3 , as evidenced by the existence of unprotonated pyridine signals (S6, SI). A similar swollen core has been confirmed in our previous study of PS-*b*-P4VP/formic acid micelles formed in chloroform at a molar ratio of formic acid/pyridine units $< 1/2$.³¹ When $t \geq 120$ h, the core was swollen by water, indicated by the appearance of the signals of protonated pyridine units. When $t = 10$ and 24 h, the $\langle D_h \rangle$ values were 159 and 153 nm, respectively. Obviously, as the intermediate state between the chloroform swollen state and the water swollen state, the core of the micelles formed at $t = 10$ and 24 h is in a less swollen state. This conclusion is supported by our TEM observations that the polymeric micelles formed at different t values in a dried state actually have a similar size as is detailed next.

The morphologies of the polymeric micelles formed at different t values were observed by TEM. The typical TEM images are presented in Figure 3. The TEM samples were prepared with great care: (1) upon dropping a droplet of the solution on the copper grid, the excess solution was wicked away. (2) The TEM samples were dried in a desiccator to prevent them from absorbing water. At $t = 0$ min, no regular aggregate was observed (S1, SI) because the block copolymer was molecularly dispersed in its common solvent chloroform. This is consistent with the result of DLS characterization at $t = 0$ (Figure 1). The aggregates formed at $t = 1$ min had a wide size distribution, and some of them were irregular in shape (S1, SI). This is also consistent with the conclusion obtained from the DLS measurements that the aggregates formed at $t = 1$ min are anomalous micelles. TEM observations demonstrate that the regular micelles were formed at $t \geq 3$ min (Figure 3a). Although DLS measurements exhibit that the $\langle D_h \rangle$ value varies markedly with an increase of t , the micelles at different t values in the dried state observed by TEM actually have a similar size and a narrow size distribution (Figure 3a–e). This supports the previously mentioned conclusion that the size differences of the micelles formed at $t \geq 3$ min detected

by DLS actually arise from the different swelling states of the core.

We noted that in the aqueous core of PMACs formed at the late periods of water and HCl diffusion, the density of the P4VP chains in the core should be low. For example, when $t = 120$ h, the weight ratio of P4VP in the core is less than 10% (Table 1). The PMACs with a core of such low density should be nearly hollow under TEM observations. However, due to the contraction of the core during the drying of the TEM samples, we cannot observe the hollow structure for PMACs formed at any of the transfer times (t). To see the hollow structure by TEM, we constructed a biphasic system of an aqueous solution of pH 1 HCl containing a potassium persulfate ($K_2S_2O_8$)/PS₁₉₇-*b*-P4VP₃₄₃ solution in chloroform at 2.0 mg/mL (the concentration of $K_2S_2O_8$ in the top aqueous phase is 1.87 mg/mL; the volume ratio of the top phase to the bottom phase and the concentration of the polymer in chloroform are the same as those of the biphasic system for forming PMACs). The aggregates formed in chloroform at $t = 120$ were observed by TEM. The hollow structure (i.e., the aggregates with a low contrast central area) can be clearly seen in Figure 3f. This is due to the noncovalent cross-linking of the protonated pyridine units by the bivalent $S_2O_8^{2-}$ ions.³⁷ After the cross-linking, the contraction of the aqueous core was restricted so that the evaporation of water from the core resulted in a hollow structure of the aggregates.

It seems that with the increase of t , the contrast of the core in the TEM images increases, indicating an increase in the amount of HCl in the core with the protonation of P4VP blocks. The Cl^- ions with a relatively high atomic number, as the counterions of protonated pyridine units, enhance the contrast.

It should be mentioned here that, in the control experiments, mixing water at pH 1 with the block copolymer solution in chloroform directly could not produce such regular PMACs in the chloroform phase. Under vigorous stirring or ultrasonic vibration, the aggregates obtained were irregular with a wide size distribution (S7, SI).

Application of PMACs as Nanoreactors to Prepare Various Inorganic Nanoparticles. As mentioned before, the PMACs attempted to combine the advantages of reverse microemulsions and polymeric micelles dispersed in a low-polarity solvent with a polar core when used as nanoreactors for preparing inorganic nanoparticles. The aqueous core of the same PMACs can load various water-soluble precursors or some hydrophobic precursors whose hydrolysis products are water soluble, and the shell can stabilize the inorganic nanoparticles formed in the core.

We first tried to synthesize silica nanoparticles in PMACs using TEOS as the precursor. In the reverse microemulsion method for preparing silica particles,³⁸ the water-insoluble precursor TEOS hydrolyzes at the oil/water droplet interface under basic or acidic conditions, followed by further condensation in the water droplets to form the silica particles. In the present study, the TEOS precursor, which is soluble and stable in the chloroform phase, was added into the PMACs solution under magnetic stirring. Similar to the case of REs, the hydrolysis reaction occurred at the interface, and the condensation reaction was restricted in the aqueous cores of PMACs, forming silica nanoparticles in the cores of PMACs (Figure 4a). The formed composite nanoparticles can be individually dispersed in chloroform. The formation of silica nanoparticles in the core of PMACs was confirmed by EDX analysis focused on an individual nanoparticle (Figure 4b). The Cu and Al elements detected come from the copper grid. The $\langle D_h \rangle$ value of the PMACs/silica composite nanoparticle characterized

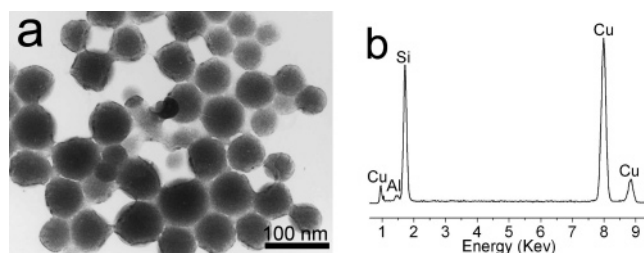


Figure 4. TEM image of PMACs/silica composite nanoparticles (a) and EDX spectrum of a PMAC/silica nanoparticle (b).

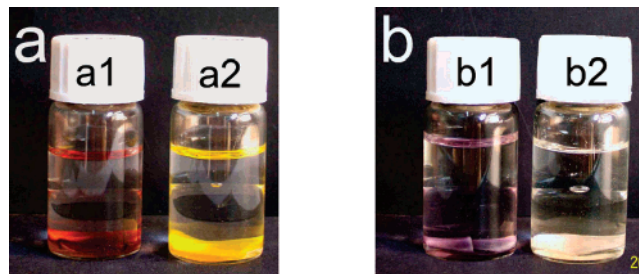


Figure 5. (a) Test paper at the bottom of a1 or a2 is a piece of filter paper soaked with $FeCl_3$ aqueous solution; the bottom phase is chloroform, and the top phase is an aqueous solution of NH_4SCN in pH 1 HCl (a1) and that in neutral deionized water (a2). (b) Test paper is starch iodide paper; the bottom phase is chloroform, and the top phase is the aqueous solution of $(NH_4)_2S_2O_8$ in pH 1 HCl (b1) and that in neutral deionized water (b2). The photographs were taken 5 h after the formation of the biphasic systems.

by DLS was 168 nm, which is much larger than the size observed by TEM. Many factors may lead to the difference between $\langle D_h \rangle$ and size observed by TEM, as explained in our previous study.³⁰

In most cases, the precursors of desired inorganic nanoparticles are insoluble in chloroform. They have to diffuse into the aqueous core of PMACs through the chloroform phase when PMACs are used as a versatile nanoreactor. It has been confirmed that HCl can diffuse into chloroform, as mentioned before. We conducted simple experiments to prove that the small amount of HCl in the chloroform phase can facilitate the transfer of inorganic species through chloroform. In Figure 5a, a piece of filter paper soaked with a $FeCl_3$ aqueous solution was placed at the bottom of a1 and a2 and covered by a 2 cm thick chloroform layer, respectively. Then, an aqueous solution of NH_4SCN in pH 1 HCl and that in neutral deionized water were added to form the top aqueous phase in a1 and a2, respectively. The filter paper in a1 became red gradually in hours, demonstrating that SCN^- could diffuse through chloroform to react with Fe^{3+} on the filter paper. The filter paper in a2, in which the top phase was formed by NH_4SCN in neutral deionized water, did not change color even after weeks. As shown in Figure 5b, starch iodide paper was used to test the transfer of $S_2O_8^{2-}$. The bottom phase was also chloroform, and the upper aqueous phase in vials b1 and b2 was the aqueous solution of $(NH_4)_2S_2O_8$ in pH 1 HCl and that in neutral deionized water, respectively. The starch iodide paper at the bottom of b1 turned purple in hours, indicating that $S_2O_8^{2-}$ in pH 1 HCl could diffuse from the top aqueous phase through chloroform to oxidize I^- on the test paper. The test paper at the bottom of b2 did not change color. Obviously, the diffusion of HCl into the chloroform phase assisted the diffusion of the inorganic compounds. The diffusion of inorganic species through the water/oil interface is a very important topic of scientific research.^{39,40} Yet, to our knowledge, the HCl-assisted diffusion of inorganic species has never been reported before (see S8, SI for experimental details).

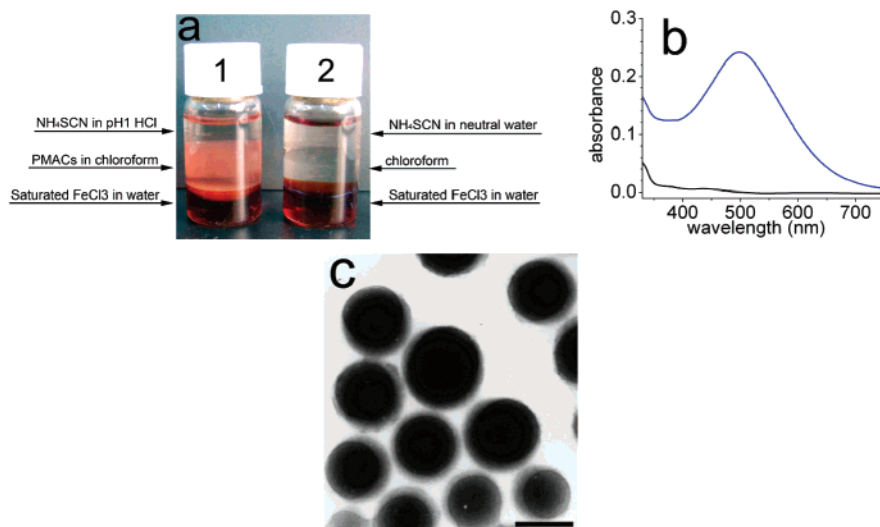


Figure 6. Digital picture of the triphase system with (vial 1) or without (vial 2) PMACs in middle chloroform phase taken after the system was standing for hours (a). UV-vis spectra of the middle chloroform phase with (blue line) or without (black line) PMACs measured after the system was standing for hours (b). TEM image of $\text{Fe}(\text{SCN})^{2+}/\text{PMACs}$ composite nanoparticles (c). The scale bar is 100 nm.

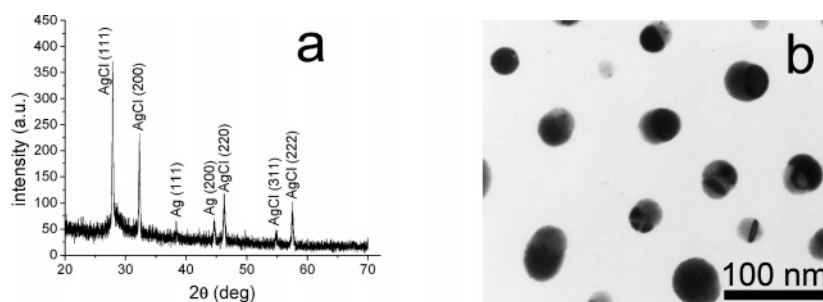


Figure 7. XRD pattern of PMACs/AgCl composite nanoparticles (a) and TEM image of PMACs/AgCl composite nanoparticles (b).

Although the existence of HCl in the chloroform phase makes the transfer of inorganic species through it to the cores of PMACs possible, whether or not PMACs can localize an inorganic reaction in the cores is a crucial point. First, we demonstrate that this bulk chloroform phase with HCl and water cannot host an inorganic reaction. A triphase system was constructed carefully as shown in Figure 6a (detailed in the Experimental Procedures). The bottom phase (in both vial 1 and vial 2) is a saturated FeCl_3 aqueous solution whose density is larger than that of chloroform; the middle phase is a PMACs chloroform solution (vial 1) or chloroform (vial 2); the top phase (in both vial 1 and vial 2) is a NH_4SCN aqueous solution containing HCl ($\text{pH} = 1$). The middle chloroform phase containing PMACs (vial 1) became red gradually in hours, while the chloroform phase without PMACs (vial 2) remained colorless. This demonstrates that the chloroform phase without PMACs cannot host the reaction between Fe^{3+} and SCN^- , whereas the reaction between Fe^{3+} and SCN^- can occur in the middle phase containing PMACs. Obviously, Fe^{3+} and SCN^- reacted in the aqueous cores, forming $\text{Fe}(\text{SCN})^{2+}$, according to EDX analysis of the components encapsulated in the cores of PMACs (S9, SI). The UV-vis spectrum of middle chloroform phase is presented in Figure 6b. The PMACs solution containing $\text{Fe}(\text{SCN})^{2+}$ in the aqueous cores showed maximal absorbance at 498 nm (blue line). The chloroform phase without PMACs (vial 2) did not show such an absorption peak of $\text{Fe}(\text{SCN})^{2+}$ (black line). The TEM image of the $\text{Fe}(\text{SCN})^{2+}/\text{PMACs}$ composite nanoparticles is shown in Figure 6c. The background of the TEM images is very clear, indicating that $\text{Fe}(\text{SCN})^{2+}$ is localized in PMACs. Otherwise, the high contrast $\text{Fe}(\text{SCN})^{2+}$ outside PMACs should have been observed in the background.

The $\langle D_h \rangle$ value of the $\text{Fe}(\text{SCN})^{2+}/\text{PMACs}$ composite nanoparticles characterized by DLS is 104 nm. As explained in our previous study, for the same particles, the $\langle D_h \rangle$ value can be larger or less than or equal to the size observed by TEM.³⁰

Jungmann et al.⁴¹ reported amphiphilic poly(organosiloxane) nanospheres as nanoreactors for the synthesis of noble metal colloids. In their method, the transfer of a hydrophilic precursor through the solvent into the nanospheres was achieved by either liquid-liquid or solid-liquid phase transfer. In the present study, we further confirm that two inorganic precursors FeCl_3 and NH_4SCN in the solid state can be introduced into PMACs at the same time and react in the aqueous cores of PMACs (S10, SI).

Additionally, under mild ultrasonication and at ambient temperature ($\sim 20^\circ\text{C}$), the AgNO_3 solid was loaded into the aqueous cores of PMACs at 2.0 mg/mL to react with Cl^- (the counterion of protonated pyridine units), forming AgCl nanoparticles within the cores. The XRD pattern (Figure 7a) demonstrates that an AgCl nanocrystal was produced. The weak diffraction peaks of Ag presented in the XRD pattern indicate the reduction of a small portion of Ag^+ by natural light irradiation. The TEM image of the composite nanoparticles (Figure 7b) shows multimorphology, due to the coexistence of extra AgNO_3 and AgCl within the same cores where the two inorganic components are phase-separated. The existence of extra AgNO_3 in the cores was confirmed by the formation of Ag_2ClNO_3 upon broad-spectrum ultraviolet irradiation, as detailed next. Obviously, the AgNO_3 is in a noncrystal state because the XRD detected no signals of AgNO_3 (Figure 7a), which should have a relatively low contrast in the TEM image (Figure 7b). The protecting polymer shells are not clearly seen

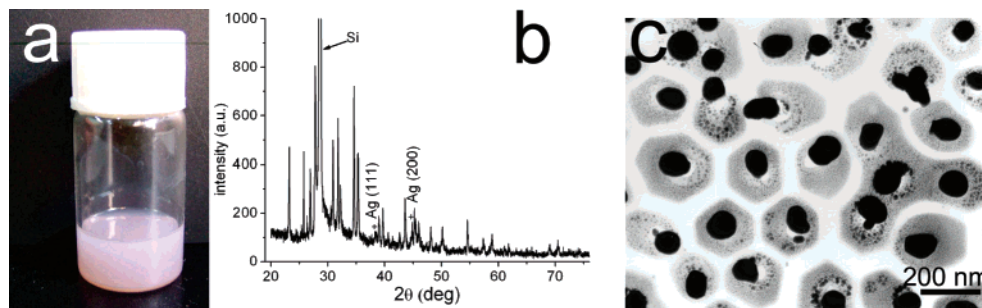


Figure 8. Digital image of $\text{Ag}_2\text{ClNO}_3/\text{PMACs}$ composite particles in chloroform containing a small amount of Ag (a), XRD pattern (b), and TEM image of $\text{PMACs}/\text{Ag}_2\text{ClNO}_3$ composite nanoparticles (c).

in Figure 7b due to their low contrast. However, the resultant composite particles can be individually dispersed in chloroform for weeks, suggesting the protection of the PS shell. The clear background in the TEM image also suggests that the amount of the inorganic compounds, which have a high contrast, outside PMACs is negligible. The $\langle D_h \rangle$ value of the $\text{AgCl}/\text{AgNO}_3/\text{PMACs}$ composite nanoparticles characterized by DLS is 144 nm. Similar to the silica/PMAC composite nanoparticles, the $\langle D_h \rangle$ value is remarkably larger than the size observed by TEM.³⁰

When the as-formed $\text{AgCl}/\text{AgNO}_3$ -containing PMAC solution was exposed to broad-spectrum ultraviolet irradiation for 5 min, Ag_2ClNO_3 was formed in the cores. From the XRD pattern after the irradiation (Figure 8b), we can see that the diffraction peaks of AgCl disappear and that those corresponding to composite salt Ag_2ClNO_3 are present. In the XRD pattern, the weak diffraction peaks at 38.38° and 44.74° can be ascribed to (111) and (200) of the cubic Ag (JCPDS Card No. 89-3722). The diffraction peak at 28.52° is attributed to the Si substrate; all other peaks are assigned to orthorhombic Ag_2ClNO_3 (JCPDS Card No. 70-2186). The formation of a small amount of Ag leads to the light purple color of the solution (Figure 8a).^{42–45} The mass ratio of byproduct Ag to Ag_2ClNO_3 was calculated to be 1.02% based on the XRD pattern shown in Figure 8b (S11, SI). Obviously, the UV irradiation leads to the formation of Ag_2ClNO_3 within the cores of PMACs. To our knowledge, only a few reports on Ag_2ClNO_3 have been published. Persson⁴⁶ prepared Ag_2ClNO_3 by saturation of a ~ 10 M aqueous solution of AgNO_3 with AgCl at about 363 K; Ag_2ClNO_3 can also be obtained by rapidly quenching a 1:1 (molar ratio) $\text{AgCl}-\text{AgNO}_3$ melt; however, no preparation of Ag_2ClNO_3 nanoparticles has been reported. The TEM image of the $\text{PMACs}/\text{Ag}_2\text{ClNO}_3$ composite particles (Figure 8c) indicates that the inorganic nanoparticles are mostly localized within the cores of PMACs. After the formation of Ag_2ClNO_3 , the phase separation between AgCl and AgNO_3 (indicated by the multimorphology seen in Figure 7b) cannot be observed in Figure 8c. These silver-containing materials may have potential applications in the biomedical industry due to their biocidal activity toward many different bacteria, fungi, and viruses and their safety toward human health.⁴⁷

Conclusion

We prepared polymeric micelles with an aqueous core (PMACs) by diffusion of HCl and water from the top aqueous phase into the bottom phase of a PS-*b*-P4VP chloroform solution. HCl molecules diffused into the chloroform, protonated the pyridine units, and drove the micellization of the block copolymer, forming micelles with a PS shell and a protonated P4VP core. Water molecules also can diffuse into and collect in the high-polarity cores. Finally, PMACs were formed and individually dispersed in chloroform. The process of forming

PMACs is well-controlled. We confirm that PMACs can be used as versatile nanoreactors to localize inorganic reactions within the aqueous cores. Our study indicates that the transfer of inorganic precursors was assisted by the existence of a small amount of HCl in chloroform. Meanwhile, the chloroform saturated with HCl and water cannot host the inorganic reaction. Various inorganic nanoparticles, such as silica, $\text{Fe}(\text{SCN})^{2+}$, AgCl , and Ag_2ClNO_3 , were synthesized within the core of the same PMACs via different mechanisms such as sol-gel, coordination, chemical precipitation, and photochemistry, respectively. We believe that PMACs can combine the advantages of reverse emulsion systems and polymeric micelles dispersed in a low polar solvent when used as nanoreactors to prepare inorganic nanoparticles.

Acknowledgment. The authors are grateful for financial support from the National Science Foundation of China (20574014 and 20528405) and for the help of Prof. Lei Zhu, University of Connecticut, in the calculation of the mass ratio of $\text{Ag}/\text{Ag}_2\text{ClNO}_3$.

Supporting Information Available: TEM images of the micelles at $t = 0$ and 1 min; ^1H NMR spectra of H_2O in CDCl_3 and in D_2O ; discussion on the three-state of water; calculation of water content in the micelles; comparison between PMACs and reverse microemulsion; preparation of $\text{Fe}(\text{SCN})^{2+}$ with solid FeCl_3 and NH_4SCN as precursors; determination of the composition of the composite nanoparticles. This material is available free of charge via the Internet at <http://pubs.acs.org>.

References and Notes

- Vriezema, D. M.; Aragonés, M. C.; Elemans, J.; Cornelissen, J.; Rowan, A. E.; Nolte, R. J. M. *Chem. Rev.* **2005**, *105*, 1445–1489.
- Forster, S.; Antonietti, M. *Adv. Mater.* **1998**, *10*, 195–217.
- Abes, J. I.; Cohen, R. E.; Ross, C. A. *Chem. Mater.* **2003**, *15*, 1125–1131.
- Bennett, R. D.; Miller, A. C.; Kohen, N. T.; Hammond, P. T.; Irvine, D. J.; Cohen, R. E. *Macromolecules* **2005**, *38*, 10728–10735.
- Spatz, J. P.; Mossmer, S.; Moller, M. *Chemistry-Eur. J.* **1996**, *2*, 1552–1555.
- Spatz, J. P.; Roescher, A.; Moller, M. *Adv. Mater.* **1996**, *8*, 337–340.
- Lu, J. Q.; Yi, S. S. *Langmuir* **2006**, *22*, 3951–3954.
- Zhang, L. W.; Niu, H. J.; Chen, Y. M.; Liu, H. F.; Gao, M. Y. *J. Colloid Interface Sci.* **2006**, *298*, 177–182.
- Capek, I. *Adv. Colloid Interface Sci.* **2004**, *110*, 49–74.
- Shchukin, D. G.; Sukhorukov, G. B. *Adv. Mater.* **2004**, *16*, 671–682.
- Kim, D. W.; Oh, S. G.; Lee, J. D. *Langmuir* **1999**, *15*, 1599–1603.
- Shi, J. Y.; Verweij, H. *Langmuir* **2005**, *21*, 5570–5575.
- Zhang, X.; Chan, K. Y. *Chem. Mater.* **2003**, *15*, 451–459.
- Zhang, M. F.; Drechsler, M.; Muller, A. H. E. *Chem. Mater.* **2004**, *16*, 537–543.
- Duxin, N.; Liu, F. T.; Vali, H.; Eisenberg, A. *J. Am. Chem. Soc.* **2005**, *127*, 10063–10069.
- Moffitt, M.; Vali, H.; Eisenberg, A. *Chem. Mater.* **1998**, *10*, 1021–1028.

- (17) Underhill, R. S.; Liu, G. J. *Chem. Mater.* **2000**, *12*, 2082–2091.
- (18) Chernyshov, D. M.; Bronstein, L. M.; Borner, H.; Berton, B.; Antonietti, M. *Chem. Mater.* **2000**, *12*, 114–121.
- (19) Bronstein, L. H.; Sidorov, S. N.; Valetsky, P. M.; Hartmann, J.; Colfen, H.; Antonietti, M. *Langmuir* **1999**, *15*, 6256–6262.
- (20) Zhu, R. P.; Wang, Y. M.; He, W. D. *Eur. Polym. J.* **2005**, *41*, 2088–2096.
- (21) Zana, R.; Lang, J. Dynamics of Microemulsions. In *Microemulsions: Structure and Dynamics*; Friberg, S. E., Bothorel, P., Eds.; CRC Press: Boca Raton, FL, 1987; pp 153–172.
- (22) Scott, C.; Wu, D.; Ho, C. C.; Co, C. C. *J. Am. Chem. Soc.* **2005**, *127*, 4160–4161.
- (23) Wu, D.; Scott, C.; Ho, C. C.; Co, C. C. *Macromolecules* **2006**, *39*, 5848–5853.
- (24) Jones, M.-C.; Tewari, P.; Blei, C.; Hales, K.; Pochan, D. J.; Leroux, J.-C. *J. Am. Chem. Soc.* **2006**, *128*, 14599–14605.
- (25) Wu, P. Q.; Siddiq, M.; Chen, H. Y.; Di, Q.; Wu, C. *Macromolecules* **1996**, *29*, 277–281.
- (26) Wang, X. H.; Goh, S. H.; Lu, Z. H.; Lee, S. Y.; Wu, C. *Macromolecules* **1999**, *32*, 2786–2788.
- (27) Yan, X. H.; Liu, G. J.; Hu, J. W.; Willson, C. G. *Macromolecules* **2006**, *39*, 1906–1912.
- (28) Zhou, Z.; Zhu, B. *Macromolecules* **1988**, *21*, 2548–2554.
- (29) Peng, H. S.; Chen, D. Y.; Jiang, M. *J. Phys. Chem. B* **2003**, *107*, 12461–12464.
- (30) Peng, H. S.; Chen, D. Y.; Jiang, M. *Langmuir* **2003**, *19*, 10989–10992.
- (31) Yao, X. M.; Chen, D. Y.; Jiang, M. *J. Phys. Chem. B* **2004**, *108*, 5225–5229.
- (32) Yao, X. M.; Chen, D. Y.; Jiang, M. *Macromolecules* **2004**, *37*, 4211–4217.
- (33) Gao, Z. S.; Desjardins, A.; Eisenberg, A. *Macromolecules* **1992**, *25*, 1300–1303.
- (34) Lusse, S.; Arnold, K. *Macromolecules* **1996**, *29*, 4251–4257.
- (35) Jhon, M. S.; Andrade, J. D. *J. Biomed. Mater. Res.* **1973**, *7*, 509–522.
- (36) Forster, S.; Zisenis, M.; Wenz, E.; Antonietti, M. *J. Chem. Phys.* **1996**, *104*, 9956–9970.
- (37) Jia, X.; Chen, D. Y.; Jiang, M. *Chem. Commun.* **2006**, *16*, 1736–1738.
- (38) Brinker, C. J.; Scherer, G. W. *Sol-Gel Science. The Physics and Chemistry of Sol-Gel Processing*; Academic Press Inc.: London, 1990.
- (39) Wu, K.; Iedema, M. J.; Cowin, J. P. *Science* **1999**, *286*, 2482–2485.
- (40) Schnell, B.; Schurhammer, R.; Wipff, G. *J. Phys. Chem. B* **2004**, *108*, 2285–2294.
- (41) Jungmann, N.; Schmidt, M.; Maskos, M. *Macromolecules* **2003**, *36*, 3974–3979.
- (42) Tian, X. L.; Chen, K.; Cao, G. Y. *Mater. Lett.* **2006**, *60*, 828–830.
- (43) Huang, H. H.; Ni, X. P.; Loy, G. L.; Chew, C. H.; Tan, K. L.; Loh, F. C.; Deng, J. F.; Xu, G. Q. *Langmuir* **1996**, *12*, 909–912.
- (44) Maillard, M.; Huang, P. R.; Brus, L. *Nano Lett.* **2003**, *3*, 1611–1615.
- (45) Scaiano, J. C.; Aliaga, C.; Maguire, S.; Wang, D. *J. Phys. Chem. B* **2006**, *110*, 12856–12859.
- (46) Persson, K. *Acta Crystallogr., Sect. B: Struct. Sci.* **1979**, *35*, 1432–1435.
- (47) Sambhy, V.; MacBride, M. M.; Peterson, B. R.; Sen, A. *J. Am. Chem. Soc.* **2006**, *128*, 9798–9808.

MA070755R